Quantitative characterization of muscle fiber by image analysis

P. Buche, David Mauron

Quantitative characterization of muscle fibers by image analysis

P. Buche, D. Mauron

Département de Mathématiques et d'Informatique, Institut National Agronomique

laboratoire de biométrie INRA associé

16, rue Claude Bernard, 75231 Paris Cédex 5, France

Abstract

The paper describes a method for measuring a set of quantitative parameters - *structural parameters* (area, perimeter, diameters, shape factors) and *parameters depending on gray-levels* (average luminance and fiber type) in muscle fiber sections. Analysis is performed on a set of serially cut, transverse sections, obtained after a biopsy. A field selected on a serial cutting set is numerized with a CCD black and white video camera. It produces a set of monochrome digital images which are the input data for a model. The method first delineates each fiber section on the image called the reference cutting, calculates the structural parameters and then attempts to follow them on the other images of the set to integrate the other desired parameters -i.e, those depending on gray-levels. The method is semi-automatic. The two main steps - fiber section extraction and fiber section following - are designed to be used on the same principle : first, a completely automatic result is computed using appropriate digital image processing; second, this result is presented to the operator in order to be interactively validated. The software called RACINE - which implements the method - has been used successfully for several years by different laboratories of the French National

Institute of Agronomic Research -INRA- on several kinds of animal muscles - pork, chicken, trout, beef, rabbit, mutton and turkey. The method allows measurements at fibre section scale on samples as large as several thousand fibres, providing improvements in speed, accuracy and statistical reliability of analyses. The main applications concern meat quality control during livestock production and genetic selection.

Keywords: Image analysis, animal production, quantitative histology, meat quality

---

1. Introduction

Meat quality control is a subject of growing interest for industrial countries where the market has reached a quantitative saturation point. The French National Institute of Agronomic Research - INRA - decided to develop research programs in this direction several years ago. In this context, biologists needed tools to acquire quantitative parameters to describe muscle from histological material in an objective manner. For example, our method has been used by biologists to analyze influence of breeding and slaughtering conditions on meat quality in Fernandez et al (1994).

Muscle is composed of fibers - 75 to 90 % of the muscle volume - and several tissues. Muscle fibers are elongated cells several centimeters long and between 20 and 100 μm in diameter. A muscle is composed of several thousand fibers organized in parallel.

Meat acidification phenomena after slaughtering have a great importance to explain meat quality and meat behaviour in industrial processing. For example, post-mortem pH evolution

explains 50% of the variability of the transformation efficiency to produce ham. To analyse meat acidification, biologists study the ATP regeneration mechanism in the fibre. ATP - adenosine triphosphate - is a molecule which contains the stock of energy of the living cell. Regeneration is done using the energy found in the food - called glycogen. The regeneration process can be done by two ways : the glycolitic and the oxidative ways.

By the glycolitic way, glycogen is transformed into lactic acid and ATP. By the oxidative way, glycogen combined with oxygen is transformed into ATP, water and carbon dioxide. After slaughtering, the oxygen way is stopped, but the glycolitic one continues to work. Due to the fact that blood circulation is stopped, the lactic acid stays in the cell. Consequently, the post-mortem regeneration process by the glycolitic way determines the meat acidification.

Biologists classify cells by histoenzymology in order to determine their behavior in ATP regeneration. Two kinds of classification are mainly used :

- revealing SDH activity on a particular cutting. SDH - succinate deshydrogenase - is an enzyme which permits to identify oxidative cells.
- revealing ATPase activity at different pH inhibiting or not inhibiting this activity according to Brooke and Kaiser (1970) or Ashmore and Doerr (1971). ATPase is an enzyme which transforms ATP in energy. On each cutting, ATPase activity is revealed for only one pH value. The classification of each fiber is obtained combining the coloration intensity measured inside the fiber section in different cuttings -i.e for different pH values. In general, 3 cuttings -i.e 3 pH values- are used to classify the fibers.

A final fiber classification is obtained integrating SDH or ATPase activities measured on contiguous cuttings realized perpendicularly to the fiber elongation axis. This is defined as a

serial cutting set - see Fig. 1. A transverse section of the same fiber can be found on each cutting of the set.

In a standard serial cutting set, 3 types of cutting are to be distinguished - see Fig. 2:

- the reference cutting used to delineate the fiber section,
- the typing colorations used to classify the fibers,
- the additional parameter cuttings revealing different chemical components. For the moment, glycogen has been most frequently analyzed because of its great importance in meat quality determination.

The biologist's requirement was to have a system which would provide cross-sectional areas and parameter cutting values for each fiber type. To extract this information from the histological cuttings, two problems needed to be solved - see Fig. 3 -:

- fiber section individualization on the reference cutting,
- fiber section following from the reference cutting to each other cutting of the set to take account of all the informations describing the same fiber.

The objective of our research is to develop a system which permits biologists to treat easily and rapidly a large sample of fiber sections in order to obtain reliable statistical results.

In this paper, a method is proposed which is based on numerical image analysis.

2. Previous research

Until now, biologists have used different techniques to solve the problem of fiber section individualization:

- A first method (Marinova et al (1991)) consists in cutting up with a chisel the fiber sections on a photograph. The fibers made of paper are then weighed and this information is converted into area using a calibration relationship between paper weight and fiber area.

- A second method consists in delineating the fiber sections on a photograph manually using a cursor on a digital tablet. This system is coupled to a computer which quantifies the areas (Dudley et al (1983), Wong (1983), Pernus and Erzen (1991)).

These two methods are used to quantify the fiber section areas but do not solve the problem of classifying fibers. Usually, each fiber is assigned to a type by a visual analysis of the photography as in Pernus et al (1986). In other cases, the coloration intensity - information used to classify the fibers - is measured by a classification based on coloration using spectrophotomicroscopy as in Bye et al (1989). The system measures the optical density inside each fiber.

All these methods allow the desired information to be quantified but they are very time-consuming because a lot of work must be done manually. Therefore, the analyzed samples are generally very small: 59 fibers in Bye et al (1989) for instance.

The development of relatively inexpensive equipment for image capture and processing has boosted the experimental work using this technique (Jain 1980; Ranft et al 1983; Henckel 1989). A video CCD camera is plugged into a microscope's photo output to obtain a numerical gray level image representing the observed field. Henckel (1989) proposes a solution for both problems: fiber section individualization and following. In the individualization step, he thresholds the gray level (0-255) image interactively to detect the inter-fiber section network on the reference cutting. Henckel makes the hypothesis that there is no distortion between cuttings. Therefore the fiber following step is only solved on very small fields - around 50 fiber sections. The inter-fiber network is stored in the overlay graphics. A classifying coloration is then put on the microscope. Under video live mode, the

operator tries to match the classifying coloration field against the inter-fiber network stored in the overlay graphics.

At the INRA, biologists desire to make experiments on large sets of samples - several thousand fibers. Therefore, it is very important to design a parameter extraction process which is as automatic as possible. Henckel's method is very interesting. The interface with the operator is well-designed, but no special effort has been made to provide automatic tools for the image analysis step. The analyzed fields are relatively small - around 50 fiber sections - because the software does not take into account local distortions between cuttings. With our method, it is possible to process greater fields - between 150 and 300 fiber sections. Manual interaction is needed only to validate automatic processing for each of the two main steps - fiber individualization and fiber following. The degree of automation of our software allowed us to carry out experiments on more than 300 000 fibers - see section 5.5.

3. Materials

The biologist carries out biopsy on the animal - a sample of 0.5 x 0.5 x 1 cm - perpendicular to the elongation axis of the fibers. The sample is then immediately frozen in liquid nitrogen and stored at -80°C until histological examination can take place. Several serial 10 μm thick transverse muscle sections are obtained from each sample with a cryostat at -20°C. For instance, for the second experiments presented in section 5.5, the biologist prepared four serial cuttings, one stained in red with azorubine - the reference cutting - , one processed according to the myosin ATPase technique following preincubation at pH 4.35, one stained for SDH activity and the last processed to reveal glycogen.

For image processing, the operational system - see Fig. 4 - consists of an optical microscope equipped with a CCD black and white camera - Sony XC77CE for instance -, an image analysis board - Datacell - and a standard workstation computer - Sun 4/75 with 48 Mb central memory and a color display - running under the Unix system and Motif window manager. The image analysis board is composed of a graphic memory, an analogue-digital converter linked to the camera and a digital-analogue converter linked to a display output - monitor - to visualize images. This board is plugged into the S-bus and driven by the workstation.

The serial cuttings are numerized sequentially. Each field is represented by a 512 x 512 pixels image. Each pixel ranges from 0 to 255, according to the luminance measured by the camera. The reference cutting is first numerized using a green filter to enhance contrast between the fiber, stained in red, and the unstained inter-fiber material. Large structures belonging to the interfiber connective tissue network of the reference stain are stored, after a rapid interactive thresholding, into a graphic memory to match roughly the other stained cuttings. Then, the operator tries to match in video live mode, as well as possible, these large structures with those present in the other stained cuttings of the set. Each serial cutting set is available as a set of images. It will be processed using the methods described in the next section to obtain the desired parameters.

4. Methods

4.1 Fiber section extraction step

The aim is to delineate each fiber section only once, on the reference cutting. On this cutting, the fiber sections are coloured in black - see Fig. 2. Finding the interfiber network - which is coloured in white - is equivalent to solving the problem of delineating each fiber section. On the image, this network can be described as a large size object (hundreds of pixels), composed of interconnected thin branches. On the whole image, the object/background contrast - i.e. network/fibers contrast - is important and the illumination intensity is homogeneous - easy to obtain with microscope lamps -. These two conditions are very important for obtaining satisfactory results with image analysis. Generally, a real effort must be made to enhance the staining quality. The azorubine staining used to reveal the interfiber network is red, therefore the operator uses a green filter to enhance the contrast between fiber and connective tissue. Lamp light intensity is interactively adjusted on the video monitor to obtain the best possible interfiber/fibers contrasts.

Based on these properties, an automatic algorithm was designed to extract the interfiber network in two steps: image thresholding and interfiber network branch closing.

4.1.1 Image thresholding

Generally, gray level distribution in the image is not bimodal. The thresholding methods based on the histogram analysis are not appropriate. Inspired by Kolher (1981), the good properties of object/background contrast and illumination homogeneity have led us to detect the luminosity on which the average gradient in the whole image reaches the maximum. For each

pixel on the image, a discrete approximation of the gradient was computed using the Sobel method. For a pixel called *:

A3	A2	A1
A4	*	A0
A5	A6	A7

with A0, A1, ..., A7, its 8 neighbours. The processes to obtain the gradient in X and Y directions are:

$$\text{grad X} = (A1 + 2\,A0 + A7) - (A3 + 2\,A4 + A5)$$

$$\text{grad Y} = (A3 + 2\,A2 + A1) - (A5 + 2\,A6 + A7)$$

The gradient amplitude is given by:

$$\text{grad}(*) = (((\text{grad X})^2+(\text{grad Y})^2)/32)^{1/2}$$

Then, for each gray level on the initial image, a computation was made of the average associated gradient, accumulating the gradient values of all the positions in the image where this gray level was observed. The threshold is chosen as the luminance associated with the maximum average gradient - see Fig. 5 -. This threshold computation is global - all pixels of the image contribute to its evaluation - which enhances the robustness of the result. The pixels of a gray level higher than to this threshold are considered as belonging to the interfiber network. Generally, 90% of the interfiber network is obtained using this technique - see Fig. 6 -. A pretreatment, applied to the initial image before thresholding, enhances the quality of

results. A histogram equalization - which is generally used to enhance the contrast for display purposes - strengthens in our particular application the contrast between fiber sections and the interfiber network.

After thresholding, the binary resulting image is not perfect. Artefacts are present in the interfiber network - dark stains due to coloration in black in Fig. 6 - and inside the fibers - freezing points in white in Fig. 6. To reduce this noise due to global thresholding, we eliminate the black connected components of size below 50 pixels - to eliminate holes inside the fiber sections. This threshold is chosen small , therefore we are sure not to eliminate connected components belonging to the interfiber network which are in general large connected components -several thousand connected pixels. In order to close the little broken branches of the interfiber network, we apply a morphological closing, see Coster and Chermant (1989), of small size (size of 2).

4.1.2 Interfiber network branch closing

At this step, the interfiber network is still not entirely detected. Some long branches - size > 10 pixels - have been lost during global thresholding. To close them, we identify in the interfiber network image the pixels where the breaks occur.These are called extremity points. To do so, the interfiber network skeleton image is calculated. Then, from each extremity point, a possible closing is sought.

1. Interfiber network skeletization - This homotopic transformation - which preserves interfiber network connectivity - simplifies the interfiber network structure. All the branches are 1 pixel width. Therefore, the extremity points are defined as pixels belonging

to the skeleton so that the sum of their 8 neighbour pixels is equal to 1 - assuming that pixels belonging to the skeleton are coded 1 and those belonging to the background 0.

2. Possible closing search - First, a short distance closing process was attempted. A point belonging to the skeleton is sought in a small rectangular neighbourhood - size 10x7 pixels - starting from the extremity point and oriented in the inertial axis of the opened branch. The opened branch is defined as the set of 8-connected pixels starting from the extremity point and ending at the first node of the interfiber network. If a point is found in this neighbourhood, a segment joining the extremity point and this point is added. After this process, a more costly long distance algorithm is used to close the larger broken branches. The idea is to follow the watershed - the central axis of the interfiber network - in the gray level image starting from the extremity point. A dynamic programming process scans some possible paths - in the direction given by the inertial axis of the branch - but keeps only the 5 best lanes, maximizing the cumulated luminance intensity in the gray level image -see Fig. 7 -. The explored lanes may be long - up to 50 pixels in length -. As in the short distance process, if a point is found, a segment joining the extremity point and this point is added.

253 4.1.3 Conclusion on the interfiber network extraction step

254

255 Global thresholding and branch closing steps are completely automatic processes. The
256 algorithm provides an interfiber network image - see Fig. 8 - that the operator may validate
257 interactively. Two cases can be distinguished:
258 1. in the first case, the interfiber network is homogeneous in thickness in the entire image.
259 Then, considering that this interfiber space is artificial - due to azorubine staining which
260 stretches the interfiber space -, the interfiber skeleton is considered as a good estimation of the
261 cell borders.
262 2. In the second case, fibers are grouped in bunches which are separated by real interfiber
263 space - interfiber tissues hierarchically organised. So the operator may merge an intermediate
264 image - called the big structure image - into the skeleton of the interfiber network image. The
265 big structure image is a cleaned binary image stored after the global thresholding used during
266 the automatic step. The operator may also use a graphic tool to delineate and fill interactively
267 the thick interfiber space

268

269 A graphic editor was also developed to add or remove branches on the interfiber network.
270 When the interfiber network is validated, the morphometrical parameters describing each fiber
271 section are computed - area, perimeter, diameter. Diameters correspond to the principal axes
272 of the fibers. These axes are the eigenvectors of the covariance matrix obtained by using the
273 pixels within the fiber as random variables. The two eigenvectors of the covariance matrix
274 point in the direction of maximal fiber spread, subject to the constraint that they are
275 orthogonal.

276

277 4.2 Fiber section following step

The aim in this step is to locate, in the other cuttings of the set, each fiber section extracted on the reference cutting. As a first approximation, fibers are considered as nearly cylindrical objects. It can be affirmed that distortions coming from the biological object - the muscle - and the experimental technology are negligible compared to the acceptable lack of precision in the fiber following step. Then, the only geometrical transformation between the reference cutting and the other cuttings to be superimposed is a combination of rotation and translation - which are the two degrees of freedom of the microscope. As shown in previous work, Buche and Camillerapp (1991), this is not sufficient, because local distortions appear between the serial cuttings, due to different reasons:

- some adipocyte cells may appear in the interfiber network in one cutting and not in the others,
- some fibers may be crushed by the cutting system,
- some fibers may be contracted or expanded by a particular staining and not by the others.

Therefore, to solve the fiber following step, it is first necessary to define a geometrical transformation model adapted to our class of images in order to follow the fiber sections as precisely as possible. Second, a method must be defined to evaluate the model parameters for a given pair of images to match.

299 4.2.1 Geometrical transformation for the fiber following

300

301 The aim in the fiber following step is to measure the luminant intensity observed in the cutting
302 to match, either in a little window - 5x5 pixels for instance - centered on the fiber's estimated
303 barycenter, or inside a little belt located in the interior border of the fiber section, depending
304 on the staining type. This is because some stainings are very homogeneously distributed
305 throughout the fiber section - ATPase for instance - and some others reveal an activity mainly
306 located on the border of the fiber - like SDH. In the first case, fiber following does not need
307 great precision. A geometrical model, which can locate the fiber section barycenter -
308 calculated in the reference cutting image - inside the fiber section on the cutting to be
309 superimposed, is sufficient. In the second case, each fiber section border - calculated in the
310 interfiber network extraction step - must be located as precisely as possible in the coloration to
311 match. Consequently, this paper proposes two global transformation models well-adapted to
312 each case.
313 When luminant intensity is measured around the fiber's estimated barycenter, we propose **a**
314 **polynomial transformation** because it can take into account one or two local distortions in
315 the image field. It is assumed that the coordinates of a set of n points on the two images to
316 match are known :

317

318 $$S_1 = \{ (X_{1i}, Y_{1i}), i \in (1,..,n) \quad \} \tag{1}$$

319 $$S_2 = \{ (X_{2i}, Y_{2i}), i \in (1,..,n) \} \tag{2}$$

320

321 where (X_{1i}, Y_{1i}) is the point in image 1 which corresponds to (X_{2i}, Y_{2i}) in image 2.

322 If one calls:

$$S_2 = \{ (X_{2i}', Y_{2i}'), i \in (1,..,n) \} \quad (3)$$

the set of points resulting from the application of the polynomial transformation to the set of points S_1, the following correspondence is given:

$$X'_{2i} = f(X_{1i}, Y_{1i}) \quad (4)$$

$$Y'_{2i} = g(X_{1i}, Y_{1i}) \quad (5)$$

with f and g two polynomial functions of degree n ($n \geq 1$).

Two independent transformations are applied in the x and y directions to leave more freedom to the model. For instance, for n=2, the f function is such that:

$$X'_{2i} = a_1 + a_2 X_{1i} + a_3 Y_{1i} + a_4 X_{1i} Y_{1i} + a_5 X_{1i}^2 + a_6 Y_{1i}^2 \quad (6)$$

The Euclidean distance between the observed points (X_{2i}, Y_{2i}) and the estimated ones (X'_{2i}, Y'_{2i}) is defined :

$$dX_i = (X_{2i} - f(X_{1i}, Y_{1i}))^2 \text{ and } dY_i = (Y_{2i} - g(X_{1i}, Y_{1i}))^2. \quad (7)$$

The coefficients a_j $(j \in (1,...,n))$ are calculated in order to minimize the global differences independently:

$$DX = \sum_{i=1}^{n} dX_i$$

$$DY = \sum_{i=1}^{n} dY_i$$

using the least squares method.

The second solution proposes **a thin plate spline transformation** which holds in the model more information about the local distortions than the polynomial transformation. This model

has been presented by Bookstein (1989) and applied on lateral cephalograms - X-rays images of the head from the side. The f and g functions are now defined as thin plate spline functions. Equation (6) is replaced by the following:

$$X'_{2i} = a_1 + a_2 X_{1i} + a_3 Y_{1i} + \sum_{j=1}^{n} w_j \; U(\left|(X_{1j}, Y_{1j}) - (X_{1i}, Y_{1i})\right|) \qquad (8)$$

where $U(r) = r^2 \log r^2$ and $\left|(X_{1j}, Y_{1j}) - (X_{1i}, Y_{1i})\right|$ is the Euclidean distance between both points (X_{1i}, Y_{1i}) and (X_{1j}, Y_{1j}).

The coefficients (a_1, a_2, a_3) and w_j $(j \in (1,\ldots,n))$ are calculated to minimize a bending energy function. The thin plate spline model is inspired by physical science. It uses a thin plate distortion model under constraints applied at different spots. This model has the property of defining the thin plate physical configuration which minimizes its bending energy. The idea is to use this model to solve a bidimensional interpolation problem. Attempts are made to find the function which permits the superimposition of the set of S_1 points to the set of S_2 points, minimizing the needed bending energy as if the discards between homologous points of S_1 and S_2 had been applied orthogonally to the image plane - considered as a physical thin plate - rather than to the image plane itself.

Write $r_{ij} = \left|(X_{1i}, Y_{1i}) - (X_{1j}, Y_{1j})\right|$ for the distance between points i and j in S_1.

361 Bookstein (1989) defines the matrices:

$$K = \begin{bmatrix} 0 & U(r_{12}) & \dots & U(r_{1n}) \\ U(r_{21}) & 0 & \dots & U(r_{2n}) \\ \dots & \dots & \dots & \dots \\ U(r_{n1}) & U(r_{n2}) & \dots & 0 \end{bmatrix} \quad , (n \times n) ;$$

$$P = \begin{bmatrix} 1 & x_1 & y_1 \\ 1 & x_2 & y_2 \\ \dots & \dots & \dots \\ 1 & x_n & y_n \end{bmatrix} \quad , (n \times 3) ;$$

$$L = \begin{bmatrix} K & P \\ P^T & 0 \end{bmatrix} \quad , (n+3) \times (n+3) ;$$

362

$$V = \begin{bmatrix} x'_1 & x'_2 & \dots & x'_n \\ y'_1 & y'_2 & \dots & y'_n \end{bmatrix} \quad , 2 \times n ;$$

$$Y = \left(V | 0\ 0\ 0 \right)^T , (n+3) \times 2 ;$$

$$W = (w_1, \dots, w_n) ;$$

363 The equation

364 $$L^{-1}\, Y = \left(W \mid a_1\ a_2\ a_3 \right)^T$$

365 permits the computation of the functions f and g coefficients :

366

367
$$\begin{cases} X'_{2i} = X_{2i} , \forall i \in (1,..,n) & (9) \\ Y'_{2i} = Y_{2i} , \forall i \in (1,..,n) & (10) \\ \sum_{i=1}^{n} w_i = 0 \\ \sum_{i=1}^{n} X_{1i}\ w_i = 0 \\ \sum_{i=1}^{n} Y_{1i}\ w_i = 0 \end{cases}$$

4.2.2 Evaluation of the model parameters

To obtain an accurate estimation of the transformation model parameters - polynomial or spline - it is necessary to find a large number of homologous points -e.g. 25 pairs of points for a degree 3 polynomial function- on both images to match. Generally, biologists seek to superimpose four serial cuttings on the reference one, which required 100 pairs for one set. This is very time consuming if done manually. To solve this problem, we have developed a method to find homologous points in images to match automatically.

Our goal in this step is to obtain homologous points, homogeneously distributed in the image to be sure to take all possible distortions into account. This step is completely automatic, therefore few erroneous couples of points are expected.

Based on these criteria, the algorithm is composed of the three following steps:

- primitive extraction in the images to match,
- matching of these primitives to generate homologous points,
- homologous points validation.

4.2.2.1 Primitive extraction on the cuttings

There are two kinds of objects in our images: fiber sections and the interfiber network. Intuitively, when the operator is searching interactively for homologous points, he very often selects intersections of branches belonging to the interfiber network. Consequently, our idea is to extract the intersections automatically on both kinds of images: the reference cutting and the cuttings to match on it.

Interfiber network extraction on the reference cutting has been explained in section 4.1. On the other cuttings of the set, the available network information is made of thin branches - as in the reference cutting - and transitions between uniform gray-level regions - see Fig. 2. A recursive edge detection filter was used (Deriche 1987) which generates an image including jumps of the gray level function. These jumps are particularly marked on thin branches and on transitions between uniform gray level regions. This new image checks the main hypothesis on which the interfiber network extraction on the reference cutting is based :

- the illumination intensity is homogenous on the whole image (because this image is the result of an edge detection filter),
- the available interfiber network information is composed of thin branches (because regions of different gray level intensities have been replaced by jumps between them).

Therefore, the same algorithm as for the reference cutting is used to obtain the available interfiber network information in the edge detection image. On both kinds of images - reference and the other cuttings - the triple points of the interfiber network skeleton which define the center of the intersections are extracted. In the following, an intersection is defined as a triple point of the interfiber network plus the three thin branches starting from it - 16 pixels long.

411

412 4.2.2.2 Matching pairs of homologous points

413

414 It is hypothesized that distortions between images can be locally assimilated to translations.
415 Then each intersection in the reference cutting is associated with a list of potential
416 homologous intersections in the cutting to match - see Fig. 9. These intersections are searched
417 in the cutting to match in a window of 64 x 64 pixels centered on the reference cutting
418 intersection - i.e. the triple point (x,y) position. To find accurate matching, two kinds of
419 information are applied : the intersection shape and the compatibility with distortion
420 information, available around the analyzed reference cutting intersection.

421

422 A shape criterion based on the calculus of the differences between matched branches has been
423 defined - see Fig. 10 -. This criterion is sensitive to angular and shape differences between
424 branches. Calling O - resp. O' - the triple point of the considered intersection in the reference
425 cutting - resp. the cutting to match - and (B_1, B_2, B_3) - resp. (B'_1, B'_2, B'_3) - its branches, O
426 and O' are superimposed and for each couple of matched branches (B_i, B'_i), the sum of the
427 square differences of the pixel coordinates is calculated :

428 $$d_i = \sum_{k=1}^{\min(L(B_i),L(B'_i))} dist_8(P_k \in B_i, P'_k \in B'_i)^2$$

429 with $L(B_i)$ - resp $L(B'_i)$ - the length of branch B - resp. B' - and $dist_8$ the D_8 distance (so-
430 called chessboard distance) between P_k ($P_k.x$, $P_k.y$) and P_k ($P'_k.x$, $P'_k.y$) - is defined as :

431 $$dist_8(P_k, P'_k) = \max(|P_k.x - P'_k.x|, |P_k.y - P'_k.y|).$$

432 This calculus is normalized - $d_i / n \leftarrow d_i$ where $n = \min(L(B_i), L(B'_i))$ - and iterated on the
433 three branches:

$$d = \sum_{i=1}^{3} d_i$$

In a first approximation, it is considered that the right solution corresponds to the couple of intersections which minimizes d. But the direct use of this criterion produces a large number of errors because genuine matching is sometimes a secondary minimum of this similarity function. To enhance this result, the decision process includes available information about the local distortion in the analyzed intersection neighbourhood. For each intersection to match, a probability is associated with each potential matching using the similarity criterion. If in the neighbourhood of the intersection, many potential matchings in a given direction with a great probability are found, the matching probability in this direction for the analyzed intersection is enhanced and the matching probability in the orthogonal direction is reduced. To implement this idea, a relaxation process inspired by Barnard and Thompson (1980) was used defining a probability initialisation, a neighbourhood interaction function and an iteration process.

For a considered intersection i in the reference cutting, an initial probability is associated with each potential matching intersection l in the cutting to superimpose. $W_i(l)$ is termed :

$$w_i(l) = 1 / 1 + s_i(l)$$

Let $p_i^0(l^*) = 1 - \max_{l \neq l^*}(w_i(l))$ be the initial probability of « no matching » for the intersection i. Baye's rule is applied to obtain an initial estimate of the probability associated with label l.:

$$p_i^0(l) = p_i(l/i) \times (1 - p_i^0(l^*))$$

$$\text{with } p_i(l/i) = \frac{w_i(l)}{\sum_{l \neq l^*} w_i(l)}$$

and l^* non matching label

Two neighbourhoods are considered :

- A spatial neighbourhood to select intersections:

  j is the neighbour of i - ie $j \in V(i)$ - if $\max(|x_i - x_j|, |y_i - y_j|) \leq D_{spatial}$

- A label neighbourhood: l' is a neighbour of l if $\max(|l_x - l'_x|, |l_y - l'_y|) \leq D_{label}$.

  l_x and l'_x - resp. l_y and l'_y - are the vectors joining the considered pair of intersections to match in x -resp. y - direction.

Two interaction coefficients are computed : q^+ which measures the compatible matchings in the neighbourhood and q^- the incompatible ones. These are defined as follows:

$$q^{+k}_i(l) = \sum_{j, j \neq i, j \in V(i)} \left[\sum_{l' \in neighbour(l)} p_j^k(l') \right] \quad for\ l \neq l'$$

$$q^{-k}_i(l) = \sum_{j, j \neq i, j \in V(i)} \left[\sum_{l' \notin neighbour(l)} p_j^k(l') \right] \quad for\ l \neq l'$$

where k represents the iteration step.

The final interaction coefficient is:

$$q_i^k = q^{+k}_i \Big/ 1 + q^{-k}_i$$

The initial probabilities are updated at each step using the interaction coefficient:

$$p_i^{k+1}(l) = p_i^k(l) \times \left[A + B \times q_i^k(l) \right]$$

where A is the regulation factor - fixed to 0.0025 - and B controls the updating speed - fixed to 2.5 -. Then, the probabilities are normalised:

$$p_i^{k+1}(l) = \frac{p_i^{k+1}(l)}{\sum_{l'} p_i^{k+1}(l')}$$

The relaxation is processed until stabilisation, reached generally after 10 iterations -see Fig. 11. The couple of matched intersections associated with the best probability is then selected but will be validated in the next step.

4.2.2.3 Validation of pairs of homologous points

The matching process generates a large number of homologous points on most images to superimpose on the reference cutting - between 100 and 300 -. These points are used to evaluate the geometrical transformation model coefficients - polynomial or spline. Models are very sensitive to erroneous homologous points - especially the polynomial model, see Fig. 12.

Therefore, it is important to check the relevance of homologous points obtained by the automatic process. Three criteria are applied to filter the homologous points:

1. Only homologous points with 0.8 matching probability score are selected.

2. Only around 100 homologous points uniformly distributed on the whole image are retained to be sure of taking into account all possible distortions.

3. The relevance of homologous points to the polynomial model is analyzed. In a first approach (Buche and Camillerapp (1991)), we eliminated aberrant homologous points according to the residues using the least squares method. If these residues were higher than a given threshold - computed according to the residues' standard deviation - we suppressed the homologous points pair corresponding to the largest residue. Then, the polynomial coefficients and residues were recalculated to detect other aberrant couples. This method is not very robust and is valid only if there are few aberrant homologous points. For this reason, a filter inspired by a robust regression method called the least-median-of-squares method was implemented - LMedS - (Meer et al (1991)) instead of the least squares method.

The goal of this method is to identify outliers in data, that is, points greatly deviating from the model. LMedS is a method that remains reliable if less than half of the data are contaminated.

514 In this method, the parameters are estimated by solving the nonlinear minimization problem:

515 $$\min \underset{1\le i\le n}{med}\, r_i^2$$

516 where med means the median value and

517 $$r_i^2 = (X_{2_i}^{'} - X_{2_i})^2 + (Y_{2_i}^{'} - Y_{2_i})^2$$

518 where $(X_{2_i}, Y_{2_i}) \in S_2$; $(X_{2_i}^{'}, Y_{2_i}^{'}) \in S_2^{'}$ as defined by Eq. 2 and 3.

519 The time-complexity of the basic algorithm is very high. If n is the number of homologous
520 points and p the number of polynomial model coefficients, then the complexity is
521 $O(n^{p+1}\log n)$, which is prohibitively large. Use was made of a random-sampling version of
522 the algorithm which reduces the time-complexity to $O(mn\ \log n)$ where m is the number of
523 p-tuples chosen randomly.

524

525 The probability P that all m different p-tuples chosen at random will contain at least one or
526 more outliers is :

527 $$P = 1 - \left[1 - \left(1 - \varepsilon)^p\right)\right]^{m}$$

528 where ε is the fraction of data contaminated by outliers. For instance, for p = 3, m = 100,
529 $\varepsilon = 0.5, \quad P = 1.59 \times 10^{-6}$, which is a very low probability.

530

531 The robust estimate of the standard deviation is:

532 $$\hat{\sigma} = 1.4826 \times \left[1 + \frac{5}{n-p}\right] \underset{1\le i\le n}{med} \sqrt{r_i^2}$$

Based on the robust LMedS model and the standard deviation estimate, homologous pairs of points $\left\{(X_{1_i}, Y_{1_i})\ ; (X_{2_i}, Y_{2_i})\right\}, i \in (1,..,n)$ are filtered as follows:

1. binary weights $\underline{w_i}$ are associated with each homologous pair of points

$$w_i = \begin{cases} 1 \ if \ \dfrac{|r_i|}{\hat{\sigma}} \leq 2.5 \\ 0 \ if \ \dfrac{|r_i|}{\hat{\sigma}} > 2.5 \end{cases}$$

2. homologous pairs having $\underline{w_i} = 1$ are considered as belonging to the assumed model, homologous pairs having $\underline{w_i} = 0$ are considered as outliers.

5. Results

This section presents the results obtained from two kinds of muscle, chicken and pork. First, the different steps of our method were applied to 20 cutting sets of chicken muscle (i.e 3763 fibers) made of 2 cuttings: 1 reference and 1 typing coloration -ATPase. Second, the method was applied to 20 cutting sets of pork muscle (i.e 3252 fibers) made of 3 cuttings: 1 reference and 2 typing colorations - ATPase and SDH.

5.1 Time consumed per set

The average number of fiber sections per cuttings set is 163 for pork muscle and 188 for chicken muscle. For pork, there are two cuttings to match on the reference, therefore the respective following correction times are referred to as b1 and b2. The complete processing

time includes automatic processing time plus interactive correction time. The results are presented in Table 1.

5.2 Error rates

The erroneous or missing branches rate is a mean rate obtained by dividing the number of erroneous or missing branches by the total number of branches for each reference cutting. The erroneous homologous points rate is obtained by dividing the number of erroneous homologous points - deleted by the operator - by the total number of automatically found homologous points. The added homologous points rate is the number of homologous points interactively added by the operator -in the fiber following step- divided by the total number of homologous points. The results are presented in Table 2.

5.3 Accuracy in the following step

The distortion models -splines and polynomial- are efficient and complementary because most of the distortions encountered are correctly estimated using one of these models. The kind of distortion in the image leads to the model choice:

- Case 1: one or two local distortions in the image

  In this case, if the homologous points are uniformly distributed in the image, the polynomial model gives a good estimation of the distortion. It has been shown in Buche and Camillerapp (1991) that a degree 3 polynomial model gives the best precision. The model precision is defined as the standard residual deviation - measured in pixels - of the homologous points. 4.43 pixels on x-axis were obtained and 4.15 pixels on y-axis. Fig. 13

shows an example which illustrates the typical use of a polynomial model. A little distortion is taken into account in the upper right corner of the image.

Unlike the polynomial model, the homologous points density must be higher for the spline model. Therefore, this model is not advised for small distortions because the operator has to add more homologous points interactively than with the polynomial model.

- Case 2: several local distortions in the image

It can be noted first that spline model offers a greater degree of liberty than the polynomial one to fit local distortions. Second, it is certain the homologous control points belong to the estimated network - cf. eq. 9 and 10. Thirdly, the network can be locally distorted by adding locally several homologous points- without disturbing superimposition in the neighbouring zones -in opposition to the polynomial model. Fig. 14 and 15 present a typical case when using the same set of control points, the thin plate spline model is clearly better than the polynomial one to fit local distortions. The costs of these improvements are:

1. the homologous points density -especially in the distortion zone- must be high to fit all the local distortions,
2. the processing time is higher for the spline model (about 30 seconds) than for the polynomial one. The performance had been estimated on a Sun Sparc 4/75 Station.

5.4 Results interpretation

1- Network extraction step

Interfiber network interative validation time and erroneous branches rates come up to biologists' expectations. However, the worse rate for chicken muscle may be explained by the presence of different noises -ignored in our model hypothesis. These noises are the results of cuttings, chemical treatments and image acquisition steps:

- Fiber sections and the interfiber network are not homogeneous in grayscale -resulting in coloration problems. Therefore, in the thresholding step, fiber sections and the interfiber network are not well detected.
- During the image acquisition stage, the illumination was not homogeneous on all the field area. This problem comes from bad thresholding.
- Fiber sections contain characterized freezing points which appear in white on the image - the same luminance as the interfiber network. This case does not disturb the thresholding because, after this step, the algorithm eliminates components which are not connected to the interfiber network. But it disturbs the long distance closings. Indeed, the dynamic programming process keeps the lanes maximizing the accumulated luminance intensities. The freezing points appear in this image and then induce erroneous closing branches.

2- Fiber section following step

The matching process gives satisfactory results:

- The low rates of erroneous homologous points prove that the robust regression method is an efficient filter after relaxation process,
- The low rates of added homologous points prove that the used primitives -intersections - are significant. Indeed, these primitives permit the matching method to find many well-distributed homologous points in the entire image.

However, as in network extraction step, the results are less satisfactory in this step for some sets of chicken muscle compared to pork. The reason is that in some chicken cuttings to match, there is less interfiber information than in swine cuttings. Therefore, the algorithm finds fewer intersections. For the relaxation process, the lower the number of intersections, the higher the probability of obtaining badly-matched intersections.

Our method was initially developed for pork muscle fibers. Consequently, the results are better for this muscle than for that of chicken. But, our method has been judged robust enough to be used on several types of muscle, such as trout, beef, rabbit, mutton or turkey.

5.5 Two examples of biological results obtained with this method

This section introduces two concrete biological applications of our method, which underline two of its significant qualities. The first one, coming from animal genetic selection, shows that the degree of method automation allows work on a very large number of samples. The second one, coming from meat quality control, illustrates that it is possible with this method to analyze differents parameters on the fibers simultaneously.

5.5.1 Comparison analysis of selected lines of chicken

Two lines of chickens sharing the same genetic origin were studied (Remignon 1993): one fast and one slow-growing. The aim of the study was the analysis of the influence of selection on the total number of fibers, myofiber types and cross-sectional areas of the different fiber types.

The experimental sampling was designed as follows:
Three muscles were studied: pectoralis major is a muscle mainly composed of glycolitic fibers; anterior latissimus dorsi is mainly composed of oxidative fibers and sartorius is a mixed muscle composed of oxidative and glycolitic fibers. Samples have been taken at 6 ages (0, 1, 3, 5, 11, 55 weeks), on twelve animals per age and per line. Three fields - 250 fibers - have been analysed per muscle, animal and age. The total number of analysed fibers was therefore around 324 000 fibers.

Different results were obtained:

1. There is a higher total number of fibers (+20%) for the fast-growing line in anterior latissimus dorsi.
2. At hatching, cross-sectional areas of the different fiber types are the same. After one week, fibers are twice as large in the fast-growing line. Thereafter, during growth, the difference remains constant between the two lines.
3. The myofiber type distribution was the same in the two selected lines.

Therefore, it seems that genetic selection for the divergent growth rates modifies the quantitative but not qualitative properties.

5.5.2 Meat quality control of pork muscles

The aim of this study (Fernandez 1993) was to observe the fall in pH in slaughtered animal's muscles, because this has a great influence on meat quality parameters like colour, water-holding capacity and tenderness. The fall of pH is mainly determined by muscle glycogen content after slaughtering. Therefore, the precise objectives were the study of the effect of a 24h-fasting and behavioral stress (meetings of pairs of animals) on glycogen variation.

Two muscles were studied: longissimus dorsi (a muscle mainly glycolitic) and semispinalis (a muscle mainly oxidative). Measures were carried out on subsamples coming from the same samples at two levels:

- a global level, using an enzymeatic method on muscle homogenates
- a detailed level, using histology and our image analysis method on muscle fibers.

The first result is a glycogen contents comparison between the two muscles using both methods - at global and detailed levels - In Fig. 16 are shown the contents of glycogen, measured in micromole per gram of fresh tissue, using the global level method. Fig. 17 shows the average luminance intensities measured on glycogen stainings using our detailed level method. The higher the luminance, the lower the rate of glycogen in the fiber. Comparing those results, a generally high level of concordance can be observed.

The second one (Fernandez et al (1994)) is an analysis of both factors - fasting and stress effects - depending on the fiber types. These original results could only be obtained at the detailed level using our method. In Fig. 18 (resp. Fig.19), four groups of average luminance

intensities are represented, measured on glycogen stainings for longissimus dorsi muscle (resp. semispinalis muscle). The first column is the total number of fibers and the three others represent the three fiber types considered (αR, αW and βR). R (for red) represents oxidative fiber type. W (for white) represents glycolitic fiber type. Subtypes for red fibers indicate the contraction speediness of fibers (α for fast and β for slow). The area percentages for each type of fiber are also given under the figures for each group.

ATP regeneration is faster in glycolitic fibers than in oxidative fibers. On the contrary, oxidative fibers are more efficient than glycolitic ones in the total amount of ATP made for one quantity of glycogen. For this reason, a red muscle like semispinalis, mainly composed of oxidative fibers, plays an important function in posture and movements under the position of rest, by contrast with glycolitic muscle like longissimus dorsi, which is mainly recruited during acute physical response. This is the reason why during fasting, semispinalis has to rely on its endogeneous substrates, glycogen, more than longissimus dorsi. This interpretation is consistent with the fact that in longissimus dorsi, there is also a trend toward an increase in glycogen luminance in red fibers (αR and βR).

As for stress effect, results are different in both muscles. In longissimus dorsi, there is a significant effect for fasted animals but not for fed animals especially in fast twitch fibers (αR and αW), which are the most active fibers during physical activity associated with aggressive interaction between animals. In semispinalis, there is also a significant effect for fed animals in fast twitch fibers and no effect on fasted animals.

To conclude with these results, we can say that the use of our method allows further examination at the fiber type level and not only at the global level.

6. Discussion

6.1 Interfiber network extraction

- In rare cases, the interfiber network result is completely erroneous. It happens for example when the background is not homogeneous. It is difficult to find a completely automatic algorithm able to generate optimal results for all types of muscles and cutting preparations. It was therefore decided to develop an interactive tool which contains classical and morphological operators -lowpass and highpass filters, opening and closing, tophat, global interactive thresholding ...- plus specific parts of the extraction step algorithm - thinning, short distance closing .... This toolbox is used in an interactive mode when the operator judges that it will be more rapid to extract the interfiber network using it rather than to correct the automatic result.
- At present, in order to make restitution of the interfiber network thickness, dilatations are applied on the interfiber skeleton and merged with the big structure image - an intermediate image stored after image thresholding in the automatic extraction step. Unfortunately, the result is not very accurate for two reasons. First, branch thickness is not homogeneous. Therefore homogeneous dilatation of the interfiber skeleton is not sufficient. Second, the gray level in the interfiber network is sometimes not homogeneous - due to freezing points for instance. Therefore, the big structure image is not useful because too many freezing points appear as belonging to the interfiber network. It would seem likely that a region growing algorithm -starting from the thin branches and stopping on gray level intensity jumps- will improve the restitution of interfiber network thickness.

6.2 The choice of the transformation model

In the case of large-scale local distortions, the poor results of the polynomial model led us to test a more appropriate one. Two approaches were considered :

- The first idea, inspired by the Adaptative Mapping algorithm -Flusser (1991)- was to subdivide the image into several regions -the subdivisions depending on local distortions-. In each region, the algorithm calculates a polynomial distortion model. After several tests, it was noted that the Adaptative Mapping algorithm generates on our class of images large scale discontinuities on region boundaries. Therefore, this method was rejected.
- The second idea was the Bookstein (1989) algorithm based on spline functions. The very interesting property of this model is the preservation of spatial continuity between regions of local distortions.

6.3 Fibers following

At present, the shape criteria used in the relaxation algorithm concern only translations. Sometimes, we observe fiber distortions including rotations. To improve the results of our algorithm, a local polynomial model will be tested to match the intersections instead of the translation model. In the relaxation method, a label will be associated with a polynomial function -instead of a vector. It will be necessary to minimize another similarity criterion between two polynomial functions of the same degree.

7. Conclusion

At present, the RACINE software is successfully used in a routine fashion by several laboratories on two kinds of muscle, pork and chicken, and gives promising results for rabbit and turkey. Positive tests have been obtained for mutton, trout and beef. The software presents strong advantages:

- firstly, it permits biologists to obtain easily in a semi-automatic way, several structural parameters characterizing each fiber section,
- secondly, thanks to its matching reliability, the software gives for each fiber section precise information extracted from cuttings to match regarding fiber types and luminances,
- thirdly, the main contribution of RACINE is that its semi-automatic aspect permits application of this software to several thousands of fiber sections, which allows reliable statistical analysis.

We think also that the localization of the computed data delivered by our software would help biologists to analyze spatial distributions of fiber types, for example, small fibers in trout muscles, which appear after hatching. Therefore, it can be interesting to analyze the spatial

distribution of fibers according to their size distribution. The biological aim is to analyze the relationship between the interfiber network texture and meat quality, tenderness for instance.

At present, for trout muscle, our software is used to follow small fiber growth after hatching. Indeed, a special semi-automatic tool has been developed based on our fiber following algorithm which permits scientists to observe the appearance or disappearance of fiber sections between two serial cuttings.

Our work will now consist in improving some parts of the software (see 6.1 and 6.3). Our goal is also to generalize the matching process -using other primitives like high curvature points-, in order to use it on other image classes for other kinds of applications as for example the matching of satellite images.

Acknowledgements

The authors wish to express their gratitude to the French National Institute of Agronomic Research and especially to the Computer Sciences Department which made funds available for this project.

References

Ashmore, C.R. and Doerr, L. (1971) Comparative aspects of muscle fiber types in different species. Exp. Neurol., 31:408-418.

Barnard, S.T., Thompson, W.B. (1980) Disparity analysis of images. IEEE Transactions on Pattern Analysis and Machine Intelligence, Vol PAMI-2, n°4, July 1980: 333-340.

Bookstein, F.L. (1989) Principal warps: thin-plate splines and the decomposition of deformations. IEEE Transactions on PAMI, Vol. 11, n°6, June 1989: 567-585.

Brooke, M.H. and Kaiser, K.K. (1970) Muscle fiber types: how many and what kind ?. Arch. Neurol., 23:369-379.

Buche,P. and Camillerapp, J. (1991) Serial cutting matching: an application to muscle fiber characterization. Proc. Eurographics'91, edited by F.H. Post and W. Barth, published by Elsevier Science Publishers B.V., September 2-6, 1991, pp 329-340.

Bye, E; Gronnerod, O; Vogt, N.B. (1989) Multivariate classification of histochemically stained human skeletal muscle fibers by the SIMCA method. Histochemical Journal, 21:15-22.

Coster, M. and Chermant J.L. (1989) Précis d'analyse d'images, Presses du CNRS, pp360-380.

Deriche, R. (1987) Optimal edge detection using recursive filtering. Proc. First international conference on Computer Vision. London, June 1987, edited by J.M. Brady and A. Rosenfeld, published by the IEEE Computer Society Publications Office.

Dudley, J.; Dayhoff, M.; Ledley, C. (1983) Muscle biopsy data acquisition and display. Proc. 7th annual symposium on Computer Applications in Medical Care, October 1983, pp 763-766. Edited by J. T. O'Neill, published by the IEEE Computer Society Publications Office.

Fernandez, X.; Lefaucheur, L.; Candek, M. (1994). Comparative study of two classifications of muscle fibres. Consequences for the the photometric determination of glycogen according to fibre type in red and white muscle of the pig. Meat Science, Vol. 41 No. 2, pp 225-235.

Fernandez, X. (1993). Contributions à l'étude des facteurs de variation de la concentration musculaire en glycogène et du pH ultime chez le porc. Relations avec les qualités technologiques et organoleptiques de la viande. Thèse en Science des aliments de l'Université de Clermont-Ferrand. Avril 1993.

Flusser, J. (1991) A fast registration of images with complex geometric distortions. SCIA 91, vol II, pp 1011-1018.

Henckel, P. (1989) Image analysis, a rapid method to determine histochemical properties of skeletal muscles including individual types. Proc. 40th annual meeting of the European Association for Animal Production, Dublin. Edited and published by EAAP.

Jain, S. (1980). Segmentation of muscle cell pictures, a preliminary study. IEEE Transactions on PAMI. vol PAMI-2, no 3, p 232-243.

Kohler, R (1981) A segmentation system based on thresholding. Computer Graphics and Image Processing 15:319-338.

Marinova, S. , Lefaucheur, L., Fernandez X., Monin P. (1991). Relationship between metabolism and glycogen content in skeletal muscle fibers of large white and Hampshire crossbred pigs. J. Muscle Foods, 3, 91-97.

Meer, P; Mintz, D; Rosenfeld, A (1991) Robust regression methods for computer vision: a review. International Journal of Computer Vision, 6:1, 59-70.

Pernus, F ; Bjelogrlic Z. and Erzen, I (1986) A computer-aided method for muscle fiber type quantification. Acta Stereol, 5/1:49-54.

Pernus, F and Erzen, I (1991) Arrangement of fiber types within fascicles of human vastus lateralis muscle. Muscle & Nerve, 14:304-309.

Ranft, P., Prewitt, J. and Fu, K.S. (1983) Segmentation of microscopic transverse section pictures of muscle tissue using a split and merge technique. Proceedings of the 6th International Conference on Pattern Recognition. Section 83, medical applications. pp 626-628. Edited by Marceli Wein, published by the IEEE Computer Society Publications Office.

Remignon, H. (1993) Contribution à l'étude histologique et biochimique des muscles dans deux lignées de poulets à croissance lente ou rapide. Thèse en Science des aliments de l'Université de Clermont-Ferrand. Décembre 1993.

Wong, Fu (1983) A parallel algorithm for muscle tissue images classification. Proc. 7th annual symposium on Computer Applications in Medical Care, October 1983, pp 751-754. Edited by J. T. O'Neill, published by the IEEE Computer Society Publications Office.

Tables

	Complete processing	Interfiber network correction	Following correction		Interactive correction
Chicken	17 min. 41 sec.	5 min. 09 sec. (a)	5 min. 58 sec. (b)		11 min 07 sec. (a)+(b)
Pork	14 min.	2 min. 39 sec. (a)	1 min. 25 sec. (b1)	2 min.24 sec. (b2)	6 min 28 sec. (a)+(b1)+(b2)

Table 1 : Time consumed per set

	Erroneous or missing branches rate in extraction step	Erroneous homologous points interactively removed rate in fiber following step		Homologous points interactively added rate in fiber following step	
Chicken	8,20 %	1,91 %		16,41 %	
Swine	4,76 %	0,12 %	0,63 %	2,45 %	2,35 %

Table 2 :Error rates. These results have been calculated comparing interactive correction of branches (resp. control points) to the branches (resp. points) number obtained after automatic interfiber network extraction (resp. homologous points extraction).

Illustrations

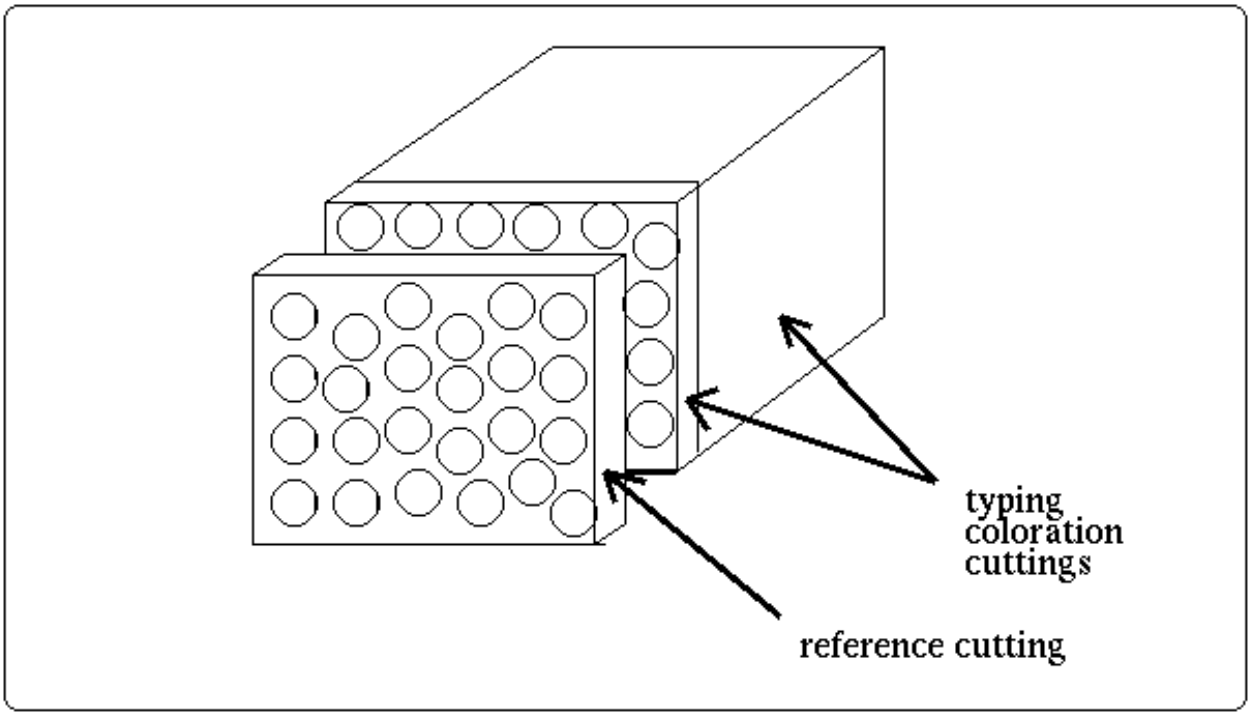

Fig. 1: Contiguous cuttings realized perpendicularly to the fiber length axis

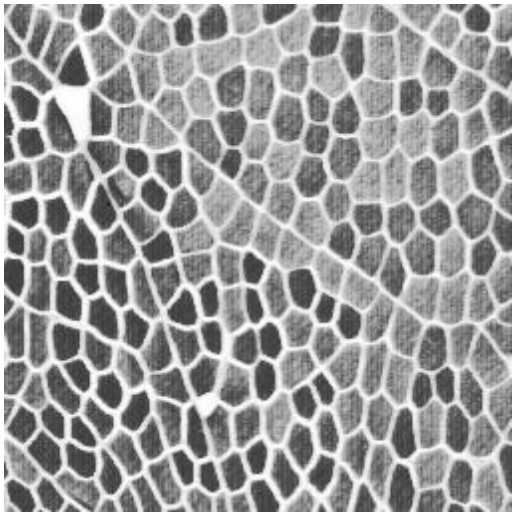

(1)

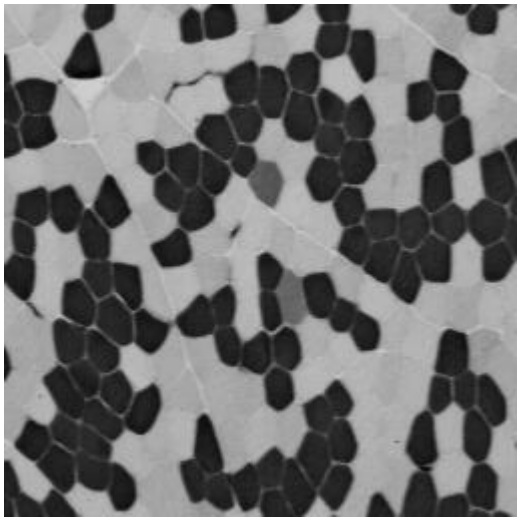

(2)

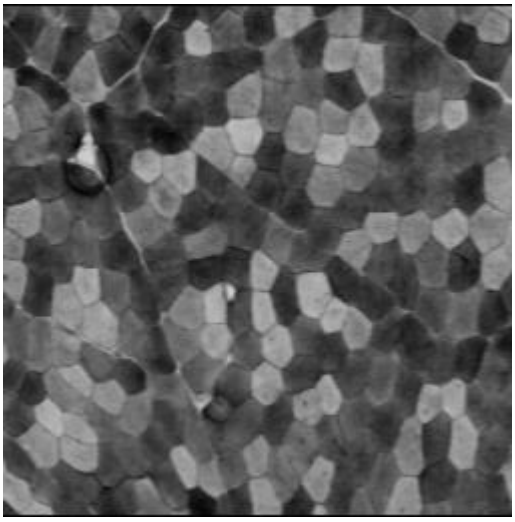

(3)

Fig. 2: A serial cutting image set: the reference cutting (1),
a typing cutting (2), a parameter cutting (3).
The size of each image is 512 x 512 pixels.

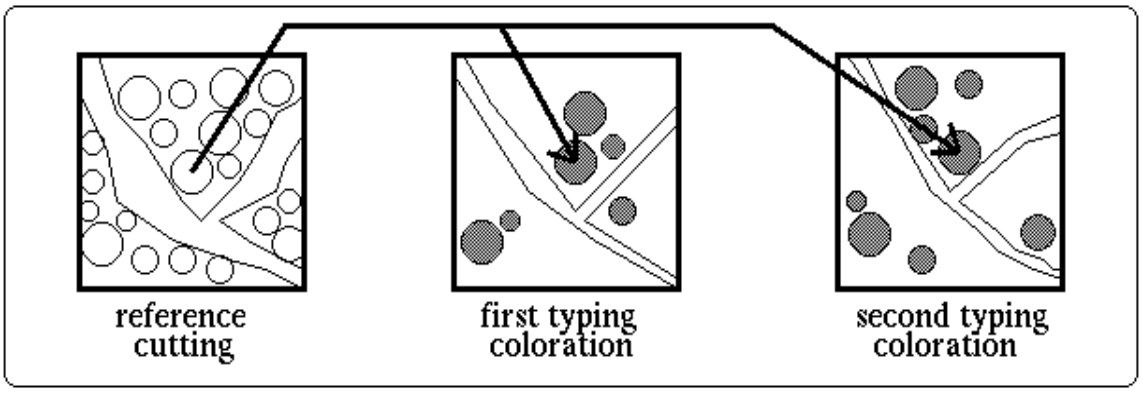

Fig. 3: Fiber following from the reference cutting to each cutting of the set

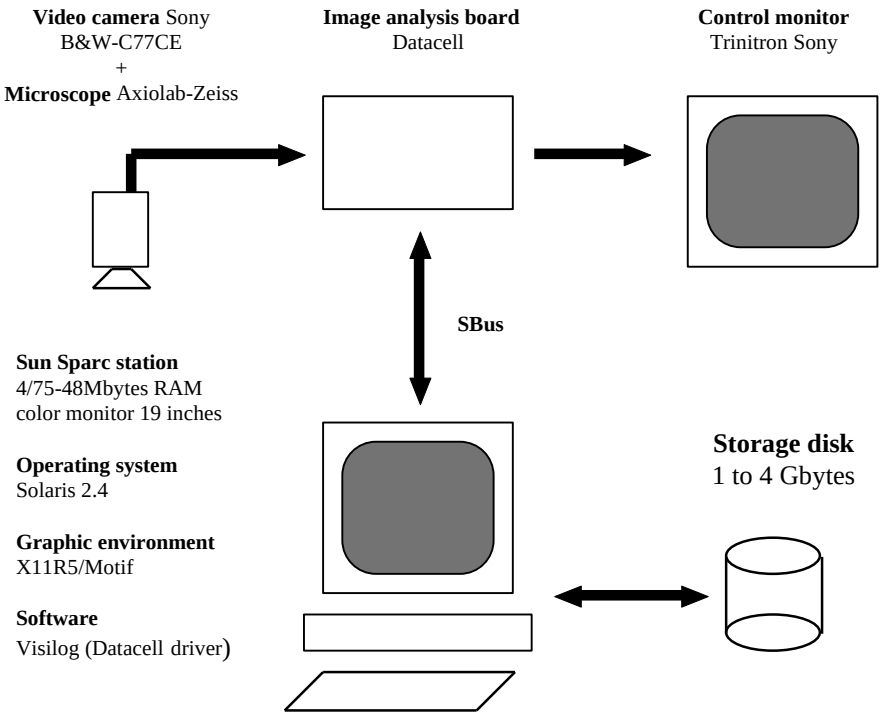

Fig. 4: Material platform required for using RACINE software.

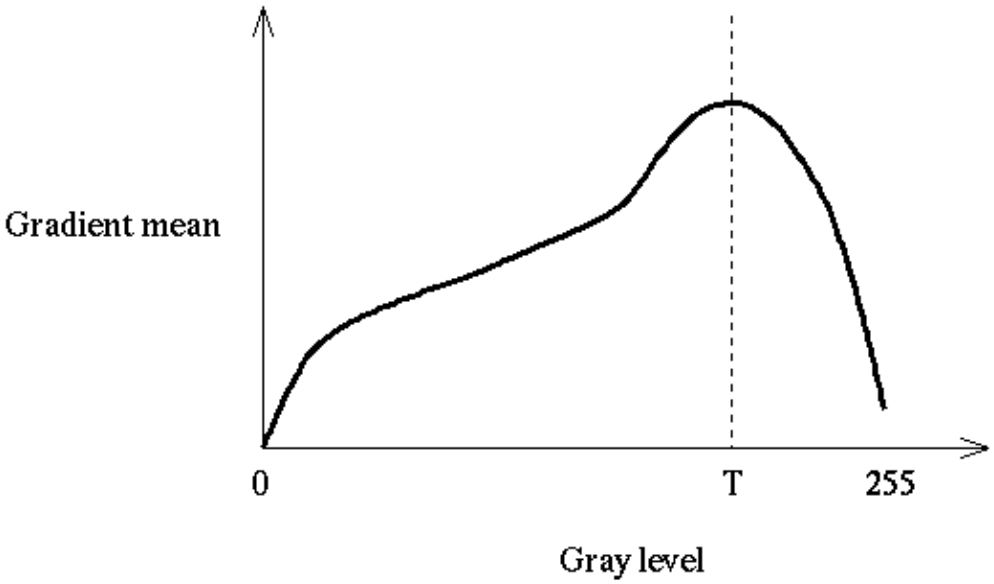

Fig. 5: Chosen threshold T in automatic extraction step.

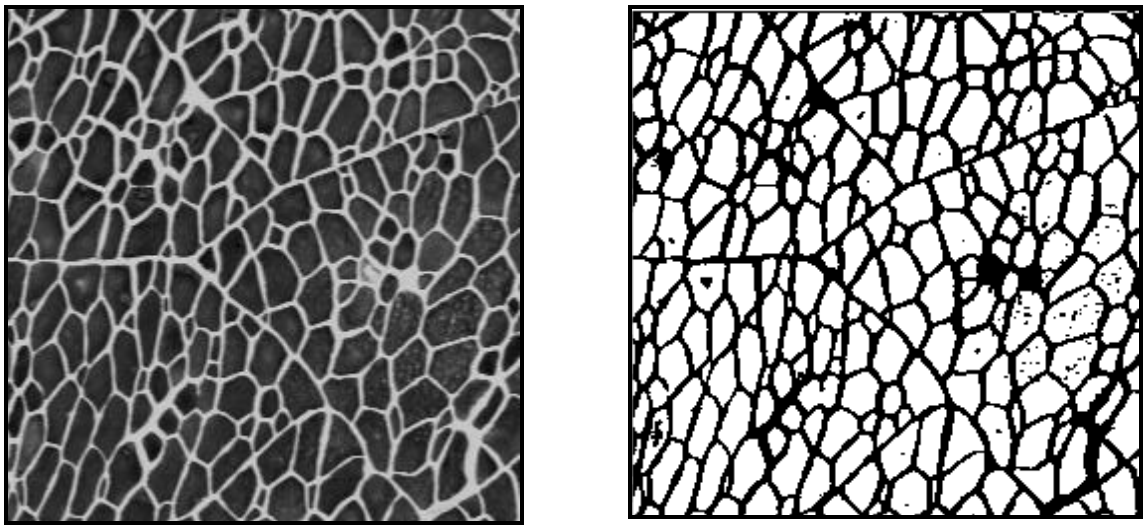

Fig. 6: Interfiber network (in white) in the initial gray level (left) image and in the binary (right) image (in black) after global automatic thresholding.
The size of each image is 512 x 512 pixels.

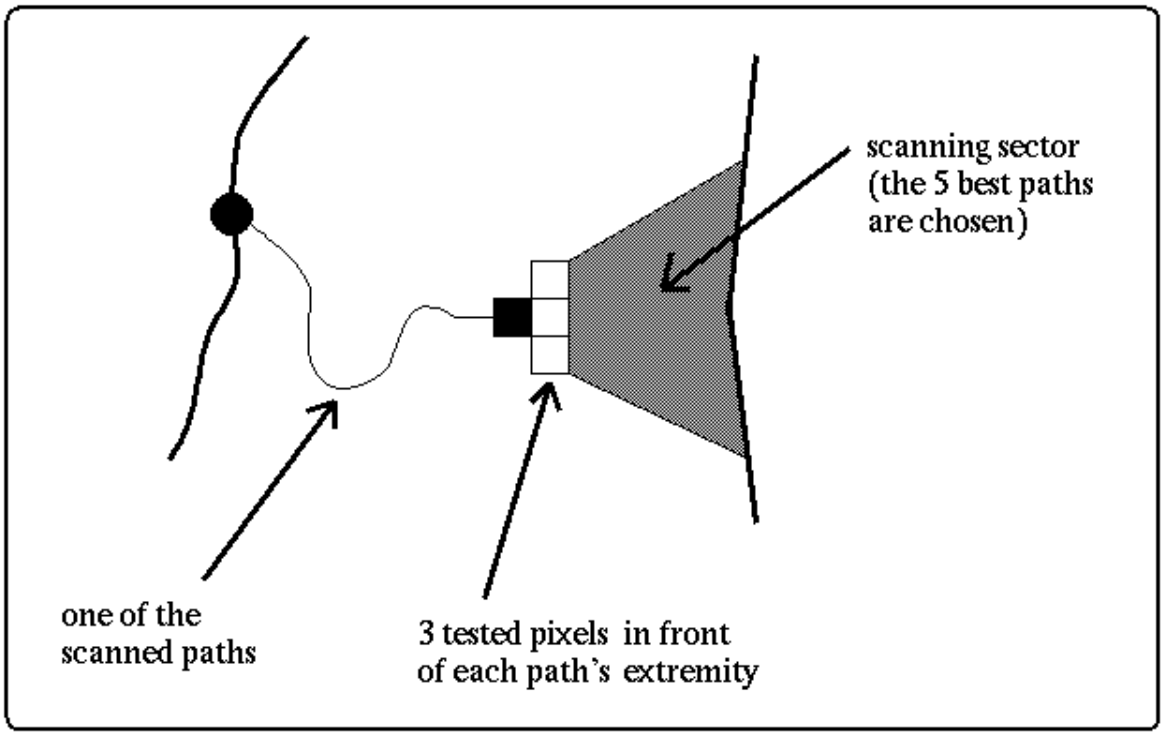

Fig. 7: Long distance branch closing step

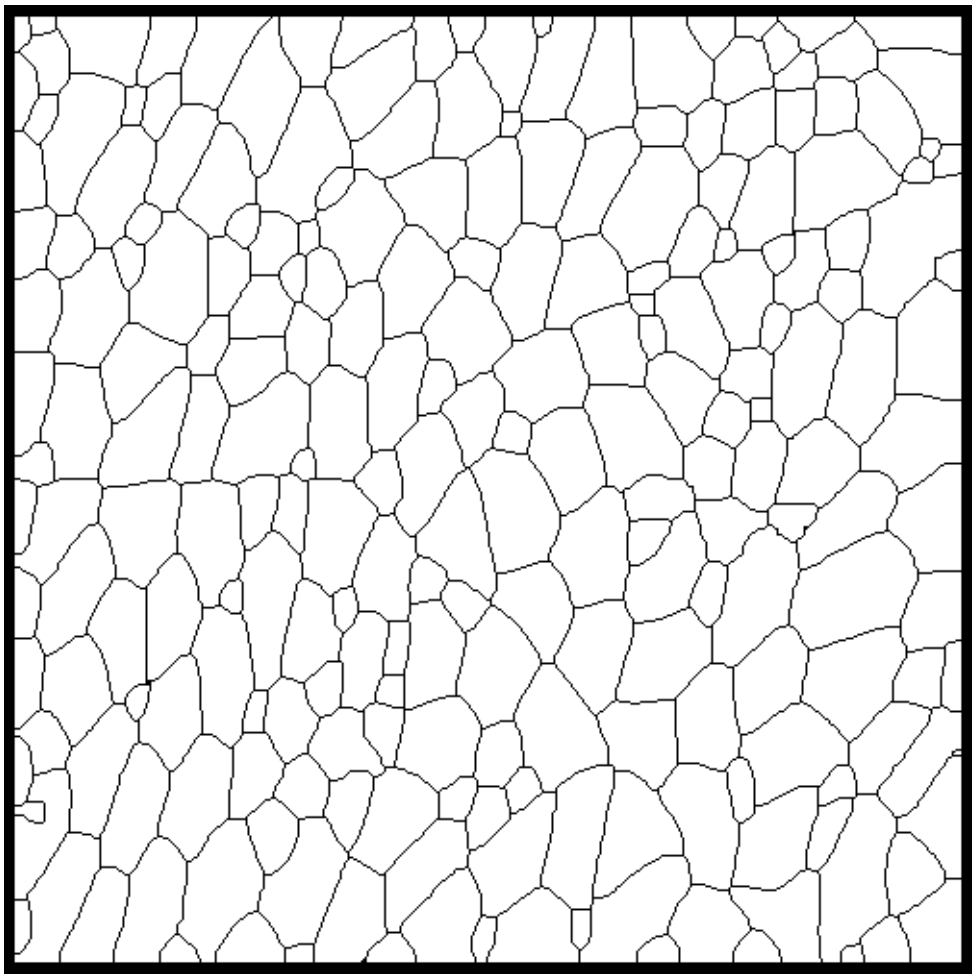

Fig. 8: Interfiber network final result - in black on the image -
The original image is the reference cutting of Fig. 6. This result is superimposed on the original image to observe and correct the network (addition or omission).

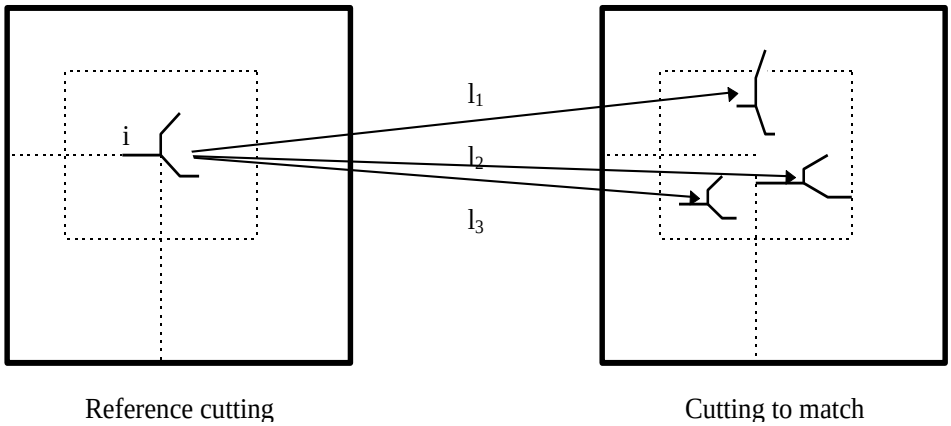

Fig. 9: The possible matchings l_1, l_2 and l_3 for the intersection i - in the reference cutting - found in a 64x64 pixels window - in the cutting to match- centered on the coordinates of the intersection i.

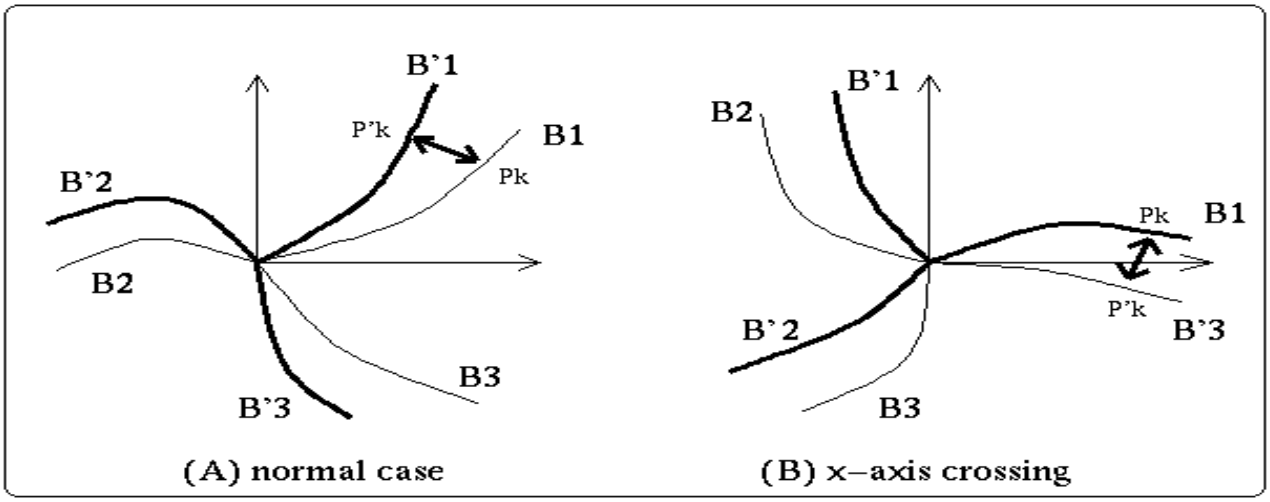

Fig. 10 : Similarity criterion between intersections.

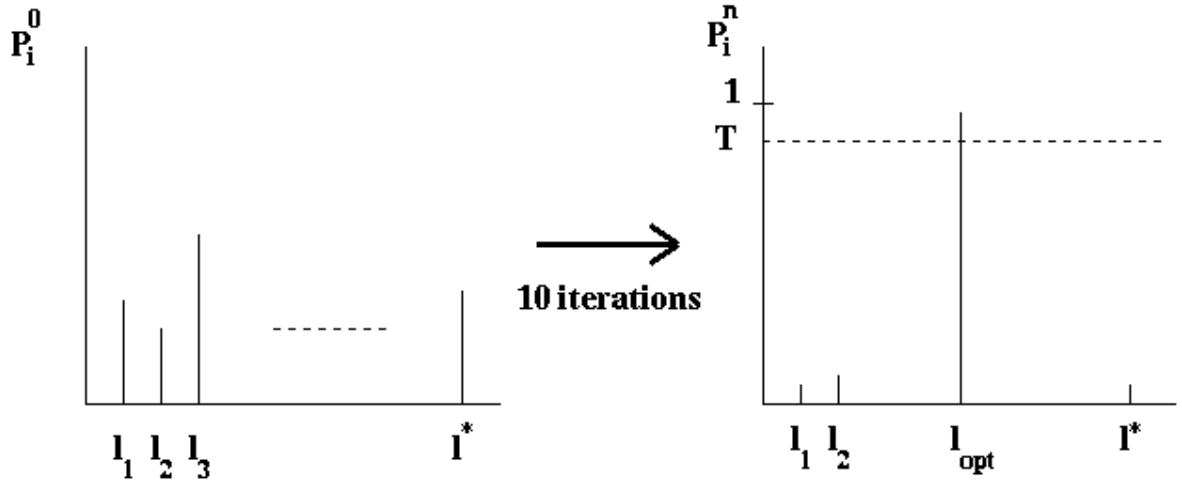

Fig. 11: Relaxation processing convergence toward l_{opt}.
The homologous pair of points corresponding to l_{opt} is selected if the matching probability score is superior to T (T=0.8 in our algorithm).

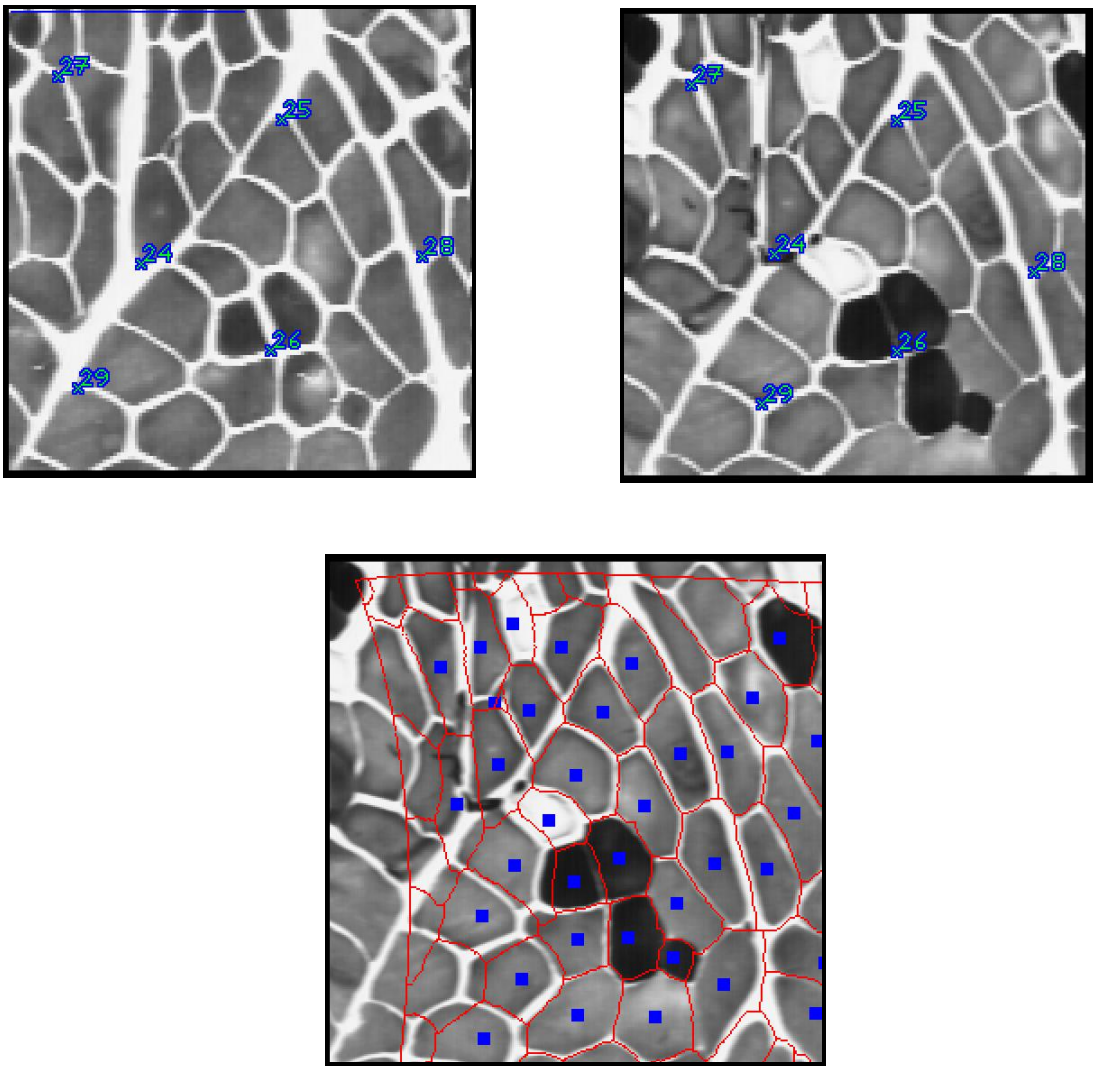

Fig. 12: The problem of polynomial transformation robustness: the interfiber network can be badly distorted by only a pair of erroneous homologous points
(here control pair of points number 29)

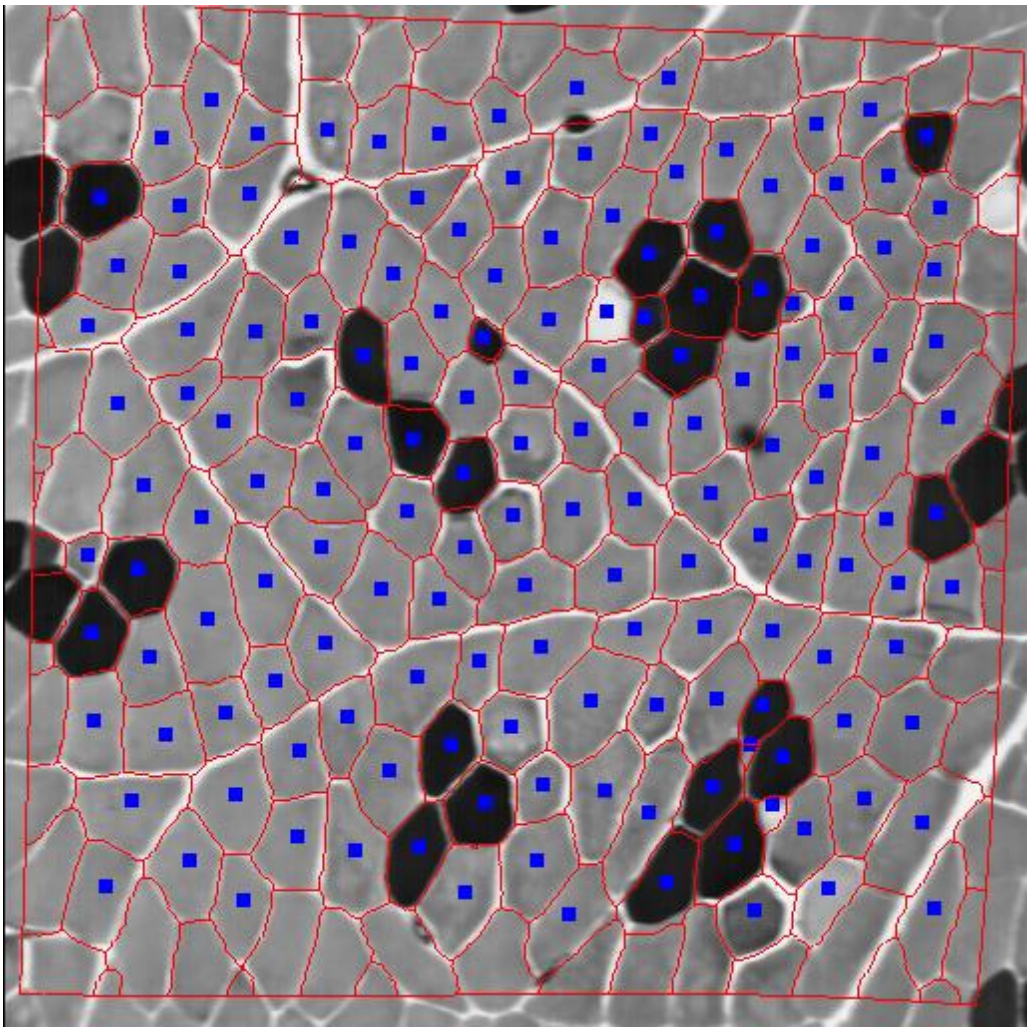

Fig. 13: Interfiber network superimposition on a cutting to match with a polynomial model

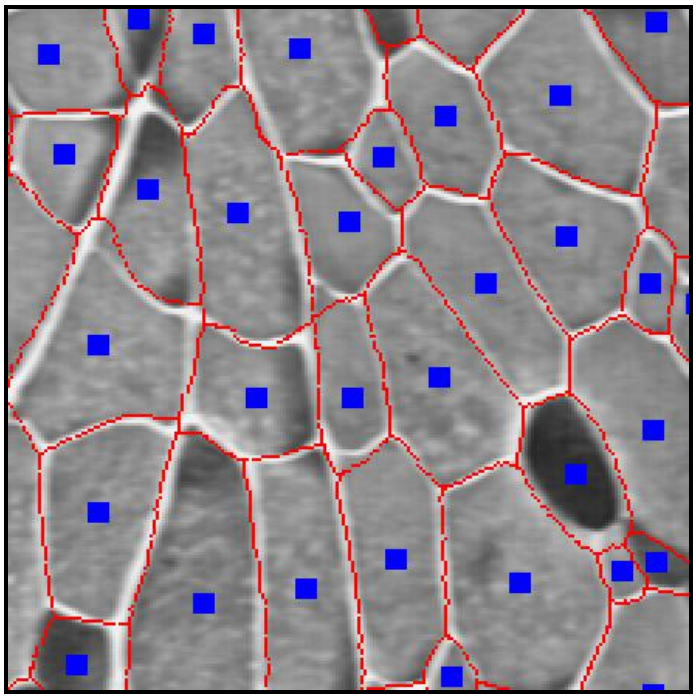

Fig. 14: Interfiber network superimposition on a cutting to match with a thin-plate spline model

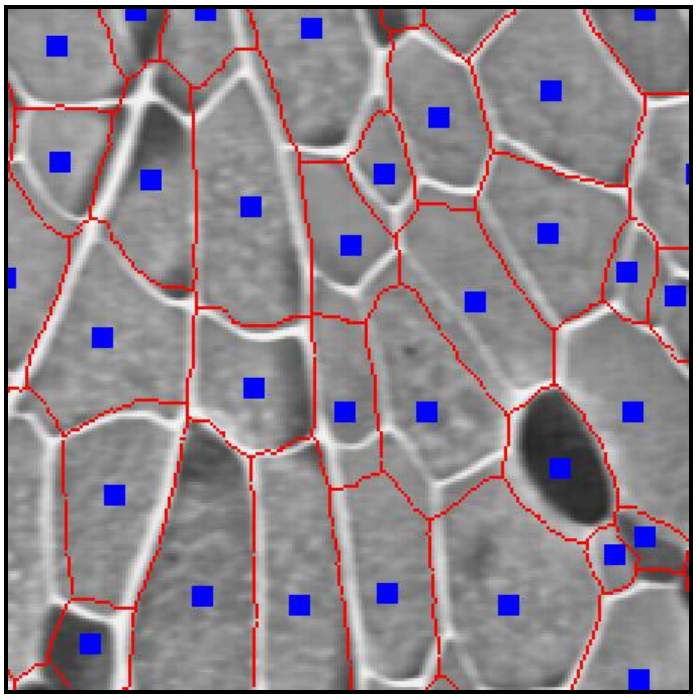

Fig. 15: Polynomial superimposition with the same control points set as in Fig. 14. The result is less accurate than with thin-plate splines

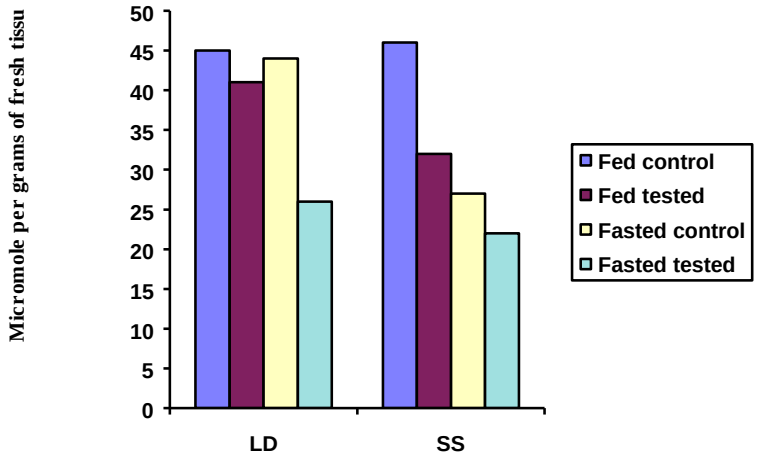

Fig. 16: Enzymeatic determination of glycogen contents
in Longissimus Dorsi (LD) and Semispinalis (SS)
- given in micromole per gram of fresh tissue -

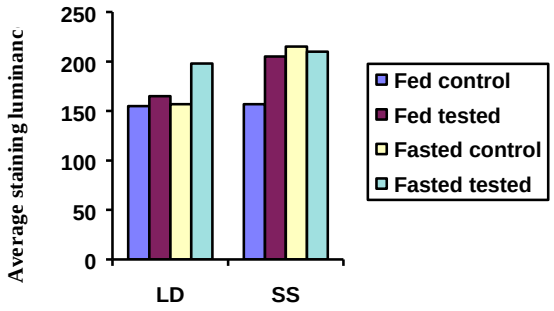

Fig. 17: Average luminance intensities measured on glycogen stainings in Longissimus Dorsi - LD - and Semispinalis - SS -

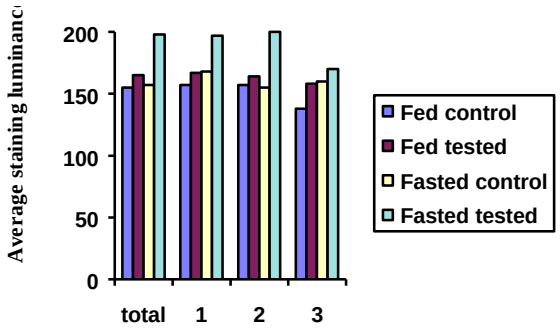

Fig. 18: Average luminance intensities measured on glycogen stainings in Longissimus Dorsi - LD - for the three types of fibers: (1) αR, (2) αW, (3) βR. The percentages of area are 14% for αR, 77% for αW and 9% for βR

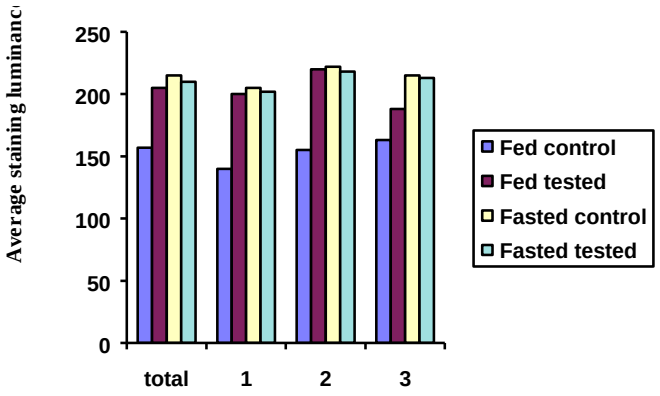

Fig. 19: Average luminance intensities measured on glycogen stainings in Semispinalis - SS - for the three types of fibers: (1) αR, (2) αW, (3) βR. The percentages of area are 19% for αR, 42% for αW and 39% for βR